Smart Sensors Network for Air Quality Monitoring Applications

Octavian A. Postolache, *Senior Member, IEEE*, J. M. Dias Pereira, *Senior Member, IEEE*, and P. M. B. Silva Girão, *Senior Member, IEEE*

***Abstract*—This paper presents a network for indoor and outdoor air quality monitoring. Each node is installed in a different room and includes tin dioxide sensor arrays connected to an acquisition and control system. The nodes are hardwired or wirelessly connected to a central monitoring unit. To increase the gas concentration measurement accuracy and to prevent false alarms, two gas sensor influence quantities, i.e., temperature and humidity, are also measured. Advanced processing based on multiple-input–single-output neural networks is implemented at the network sensing nodes to obtain temperature and humidity compensated gas concentration values. Anomalous operation of the network sensing nodes and power consumption are also discussed.**

***Index Terms*—Air quality ($AirQ$), embedded Web server, neural network, wireless networks.**

I. Introduction

AIR supplies us with oxygen that is essential for our bodies to live. Air is 99.9% nitrogen, oxygen, water vapor, and inert gases. Human activities can release substances into the air, some of which can cause problems for humans, plants, and animals.

Air quality can be expressed by the concentration of several pollutants such as carbon monoxide (CO), sulphur dioxide, nitrogen dioxide, and ozone. The threshold values specified by the European Environment Agency [1] for these pollutants are 10, 350, 40, and 120 μg/m^3, respectively.

Pollution also needs to be considered *inside* our homes, offices, and schools. Some of these pollutants can be created by indoor activities such as smoking and cooking. Generally, in industrialized countries, the population spends about 80%–90% of time inside buildings and is therefore exposed to harmful indoor pollutants. Indoor air quality is generally assessed by separately measuring CO, temperature, and humidity [2]. This information, even if fused, is insufficient to allow a good characterization of indoor air quality.

The development of wireless local area network (WLAN; IEEE802.11X) technology and the marketing of low-cost access points (APs; e.g., Linksys WAP11), wireless network adapters (CardBus; e.g., D-Link DWL-G650+), and wireless bridges (e.g., DWL-810+) creates the possibility of implementing indoor/outdoor air quality monitoring networks characterized by high flexibility, modularity, and low cost.

Tin oxide sensors (e.g., Figaro, Nemoto [3]) are inexpensive and fair selective gas sensors. To overcome some of their limitations such as cross sensitivities [4], [5] and a temperature and humidity dependence behavior [6], appropriate sensor data processing is required.

The aim of this work is to present a Wi-Fi indoor—outdoor air quality monitoring network that combines the capabilities of tin oxide sensors with advanced sensor data processing based on multilayer perceptron neural networks for an accurate measurement of air quality and for the detection of air pollution events and of sensors' abnormal operation.

II. Direct and Inverse Modeling of the Sensors' Characteristics

The sensors' nonlinearity requires the utilization of direct and inverse modeling for sensor calibration and on-line measurement phase [7]. For the particular case of tin oxide gas sensors TGS800, TGS822, TGS842, and TGS203, the sensors' response is strongly dependent on parameters such as temperature, humidity, and cross influence of the other gases. For practical and economic reasons, the number of calibration points is very low, and thus, a neural network (multilayer perceptron architecture), which is a global approximator of multivariable characteristics [8], was used in this paper. Polynomial modeling is another solution for multivariable characteristics modeling. Representative of this type of solution is the polynomial model that is a part of the IEEE1451.2 standard for smart sensors particularly related to smart sensors correction engine implementation [9]. The method represents an interesting solution. However, it requires a large set of data (i.e., a higher number of calibration points compared with a neuronal network model) for polynomial model coefficients calculation [10], i.e.,

$$\sum_{i=0}^{D(1)}\sum_{j=0}^{D(2)}\cdots\sum_{p=0}^{D(n)} C_{i,j,\ldots,p}[X_1-H_1]^j[X_2-H_2]^j\cdots[X_n-H_n]^p \tag{1}$$

where X_n are the input variables to the sensor characteristic block, H_n are the offsets to the input variables, and the $D(k)$ represents the degree of the input X_k, i.e., the highest power to which $[X_k - H_k]$ is raised in any term of the multinomial. The

Manuscript received July 3, 2007; revised October 21, 2008. Current version published August 12, 2009. This work was supported by Programa Operacional para a Sociedade da Informação through Project SFRH/BPD/11549/2002.

O. A. Postolache and J. M. Dias Pereira are with the Instituto de Telecomunicações, Lisbon 1049-001, Portugal, and also with the Escola Superior de Tecnologia de Setúbal, Instituto Politécnico de Setúbal, Estefanilha 2910-761 Setúbal, Portugal (e-mail: poctav@alfa.ist.utl.pt; joseper@est.ips.pt).

P. M. B. Silva Girão is with the Instituto de Telecomunicações, Lisbon 1049-001, Portugal (e-mail: psgirao@ist.utl.pt).

Color versions of one or more of the figures in this paper are available online at http://ieeexplore.ieee.org.

Digital Object Identifier 10.1109/TIM.2009.2022372

$C_{i,j,\ldots,p}$ represent the calculated correction coefficients for each term values that are obtained, considering the segmentation of the input variable range. The accuracy of the method is influenced by the polynomial degree, the number of segments, and the number of values included in defined subranges that make the multivariable polynomial inverse modeling for external factors compensation computationally expensive. Considering only one segment for a given gas concentration, where the voltage acquired from gas sensor channel represents the primary variable $(X_1 = V_{G_i})$, and restricting the number of influence factors on gas concentration measurement to temperature and humidity expressed by voltage values acquired from temperature and relative humidity sensor channels $(X_2 = V_T, X_3 = V_{RH})$, the compensated values of gas concentration C_{G_i} are expressed by

$$C_{G_i} = C_{000} + C_{100}C_{G_i} + C_{010}V_T + C_{001}V_{RH} + C_{101}V_{G_i}V_{RH} + C_{110}V_{G_i}V_T + C_{011}V_TV_{RH} + C_{111}V_{G_i}V_TV_{RH}. \quad (2)$$

As can be observed, to reduce the complexity the first-degree polynomial approximation is considered. Better accuracy can be obtained with a higher degree multivariable polynomial model, which implies an increase of the computational load. A comparison between the "classical" polynomial modeling and neural network modeling shows that the number of calibration points used to calculate the polynomial coefficients for an imposed accuracy of inverse characteristic modeling is generally greater than the number of calibration points used to design the neuronal network sensor models [11]. Moving the complex processing from the embedded server to the Web browser side permits us to overcome some of the drawbacks of neural network processing such as the high number of multiplication and the use of nonlinear transfer functions (e.g., $\tanh(\cdot)$).

III. Sensors' Network

Gas sensor networks provide a promising mechanism for mining information from the monitored areas. The following two types of Wi-Fi (WLAN) architectures were considered: 1) an ad hoc architecture and 2) an AP infrastructure network, which assures additional services (e.g., data publishing on the wired Internet), taking into account that the AP works like a bridge between the wired and wireless network [12]. The ad hoc architecture seems to be a good solution, particularly for air quality monitoring in outdoor conditions since it requires less elements and, thus, less power consumption.

The ad hoc smart sensor network (Fig. 1, case 1) includes the following three elements: 1) a PC with an IEEE802.11g-compatible Wi-Fi cardbus adapter (DWL-G650+) as the main control and processing unit; 2) a set of sensing nodes (SN_j) with air quality sensors $(\mathrm{GS}_1, \mathrm{GS}_2, \ldots, \mathrm{GS}_i)$; and 3) a data acquisition, primary processing, and transmission control protocol/Internet protocol (TCP/IP) communication unit (APC) based on IPμ8930 general-purpose network controller whose Ethernet port is connected to a DWL-G810 wireless bridge.

Referring to the AP infrastructure (case 2), the wireless network node components are the same as that of case 1, with the only difference being the inclusion of an AP (LinksysWAP11), which is an element that extends the wireless subnetwork

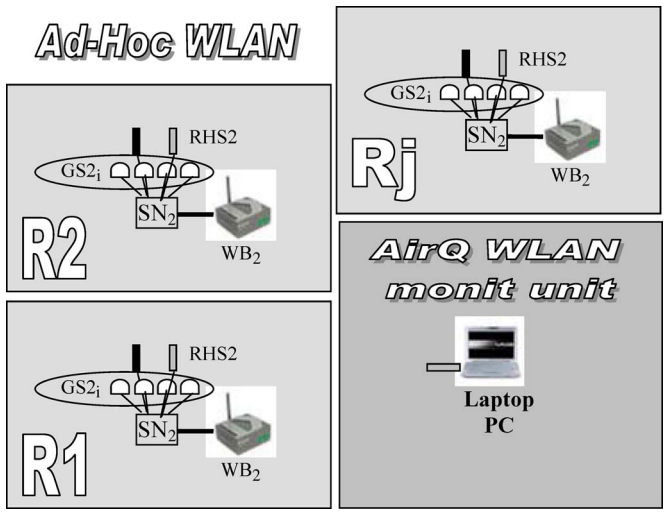

Fig. 1. Ad hoc air quality smart sensor network architecture associated with different rooms (R1, R2, . . ., Rj), where SN_j are sensing nodes, $\mathrm{GS}_{j\,i}$ are gas sensors, TS_j are temperature sensors, RHS_j are relative humidity sensors, and WB_j are wireless bridges.

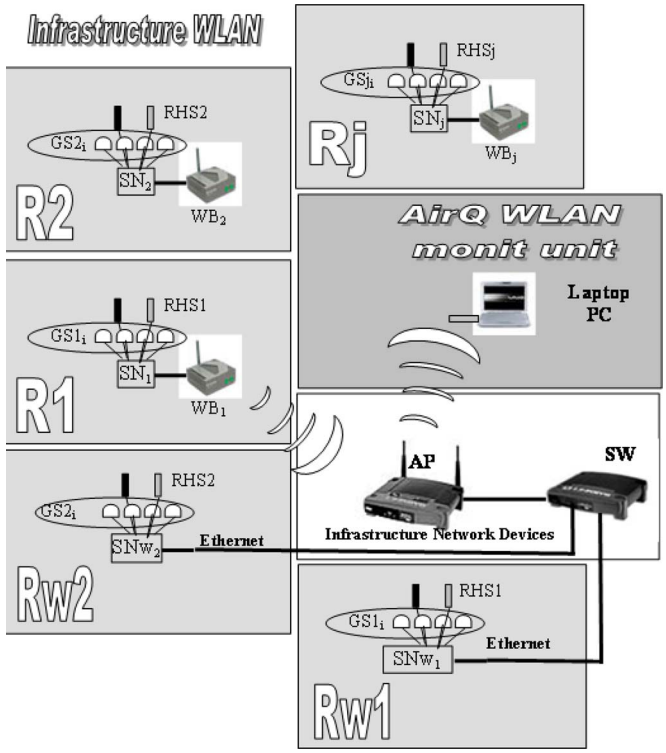

Fig. 2. Infrastructure WLAN air quality smart sensor network architecture that includes sensing nodes distributed in different rooms. R1, . . ., Rj: Rooms with wireless sensing nodes. Rw1 and Rw2: Rooms with wired sensing nodes. SN_j: Sensing nodes. $\mathrm{GS}_{j\,i}$: Gas sensors. TS_j: Temperature sensors. RHS_j: Relative humidity sensors. WB_j: Wireless bridges. AP: Access point.

range capabilities and enables wireless network traffic to be transmitted over the wired network that can include additional wired sensing nodes (SN_j) distributed in different rooms (Rw_j rooms; Fig. 2).

As can be observed in Fig. 2, the wireless or wired sensing nodes are installed in different rooms (R1, R2, . . . , Rj, Rw1, Rw2, . . . , Rwj), where different values of temperature, relative humidity, and air quality are measured. Fig. 3 underlines the differences between the measured air quality parameters in the

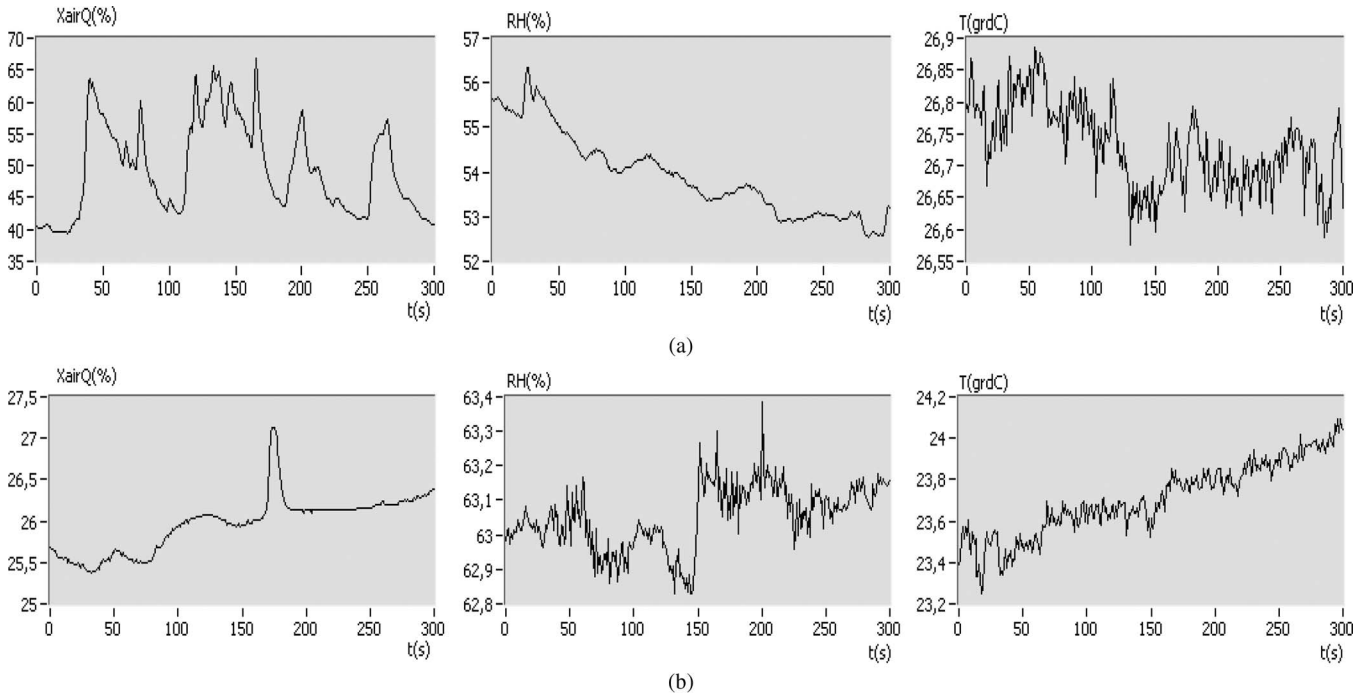

Fig. 3. Time evolution of indoor air quality parameters in two different rooms. (a) Smoking room. (b) Non-smoking room.

following two different situations: 1) smoking room and 2) non-smoking room.

A. Sensing Nodes

The sensing nodes are designed and implemented to perform the air quality ($AirQ$) monitoring using low-cost gas sensors and, at the same time, to get the additional information about the temperature T and relative humidity RH. This information is used to increase gas concentration measurement accuracy performing the error compensation caused by temperature and humidity influence.

The used gas sensors are sintered using SnO_2 semiconductor heated sensors provided by Figaro [13] that assure pollution event detection (TGS800-general air contaminant sensor-AC), methane detection (TGS842-M), alcohol and organic solvent detection (TGS822-SV), and CO detection (TGS203-CO). Information about temperature and relative humidity are obtained using Smartec SMT160-30 [14] and Humirel HM1500 [15] temperature and relative humidity transducers, respectively.

The sensor experimental direct characteristics are expressed by voltages obtained at the gas sensor conditioning circuit output for different concentrations of gas, expressed in parts per million. The used conditioning circuit for the air pollution sensor TGS800, solvent vapors (TGS822), and methane sensor (TGS842) are presented in Fig. 4.

To perform the sensor characterization, each of the considered gas sensors (GS_i) is separately introduced in a test chamber as part of a laboratory-developed gas sensor calibration system. The values of gas concentration are imposed using a mass flow controller (MC Alicat Scientific) connected to gas bottles with standard concentration (e.g., 100 ppm CO).

Temperature and humidity are measured using the temperature and relative humidity sensors that are also included in the chamber. Different values of temperature and relative humidity

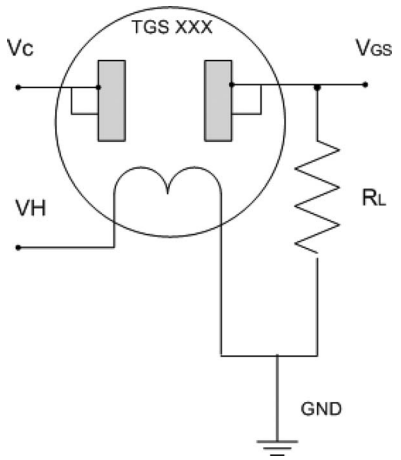

Fig. 4. Gas sensor conditioning circuit. V_c: Circuit voltage. V_H: Heater voltage. $V_{\rm GS}$: Gas sensor output voltage. $R_{\rm L}$: Load resistance.

are imposed employing a set of drying and saturation chambers connected to the testing chamber and air pumps (Fig. 5).

To decrease humidity, the drying chamber with two Peltier cells is connected to the test chamber. After condensation on the Peltier cells surface, the condensed liquid in the drying chamber is collected and pumped off from the drying chamber. Low values of relative humidity can be obtained in this way (e.g., $RH = 20\%$). Higher humidity values are obtained when the saturation chamber is connected to the testing chamber. In this case, condensed/distilled water is pumped from the water tank and vaporized into the air circulation system. Values of 95% were reached using this procedure. Using the RH variation procedure, gas sensors characteristics for $RH_1 = 35\%$, $RH_2 = 65\%$ and $RH_3 = 95\%$ were obtained.

For temperature, a Peltier cell is employed. Additionally, a testing chamber ventilator is used to inject the cold or warm the air in the testing chamber. For the considered case, several

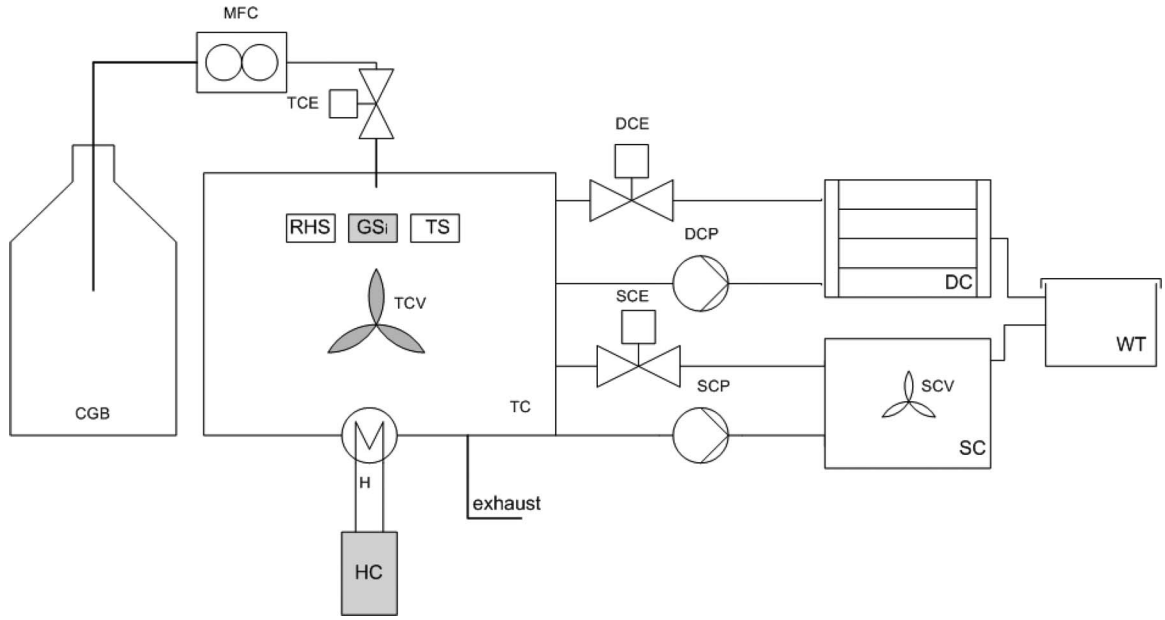

Fig. 5. Gas sensor calibration system architecture. CGB: Calibration gas bottle. MFC: Mass flow control. TCE: Testing chamber electrovalve. DCE: Drying chamber electrovalve. SC: Saturation chamber electrovalve. DCP: Drying chamber pump. SCP: Saturation chamber pump. DC: Drying chamber. SC: Saturation chamber. HC: Heater control. H: Heater. WT: Water tank. TCV: Testing chamber ventilator. SCV: Saturation chamber ventilator.

values of temperature were imposed, $T_1 = 10\ ^\circ\text{C}$, $T_2 = 15\ ^\circ\text{C}$; $T_3 = 20\ ^\circ\text{C}$, $T_4 = 25\ ^\circ\text{C}$ and $T_5 = 30\ ^\circ\text{C}$.

A gas exhaust circuit is used to clean the testing chamber after a particular gas sensor testing (e.g., TGS842 Methane gas sensor testing).

B. APC

The voltages obtained from sensors' channels are applied to the analog inputs of the APC, which is a general-purpose network controller and Web server (Ipsil IPμ8930). It performs sensing channels data conversion (voltage to gas concentration in parts per million, voltage to temperature in degrees Celsius, and voltage to relative humidity in percent) and Web data publishing (case 1) or transmits the data using TCP/IP communication to the main processing and control unit (laptop PC) that performs the data logging, data processing, and Web publishing through a LabVIEW Web server (case 2).

IV. Data Processing

Two types of sensor data processing architectures that allow the calculation of several air quality values are implemented using JavaScript and LabVIEW Web publisher technologies. The first one is a neural network algorithm implemented in JavaScript in the embedded server (Web sensor) and represents one of the main novelties of the work. The second software architecture is implemented in the network PC and performs the following three tasks: 1) sensing nodes data reading through TCP/IP remote control; 2) air pollution events detection and gas concentration estimation based on neural network inverse models of gas sensors; and 3) data logging and Web publishing of air quality data. The LabVIEW capabilities were used for the implementation of this architecture.

JavaScript is associated to the smart sensor network and assures independent dynamic webpages generation. The sensor nodes (SN_j), which are supported by embedded Web server architectures, acquire and process the voltages from sensors' channels using a set of implemented JavaScript functions (JS_i) that are part of hypertext markup language (HTML) files stored in an embedded Web server (Ipsil IPμ8930) electrically erasable programmable read-only memory (EEPROM). JS_i complexity depends on the associated sensor. Data processing is performed mainly at the Web browser level, which reduces the computational load associated with embedded Web servers and is also important as regard power consumption and Web server autonomy.

Referring to the JS_T and JS_{RH}, which are JavaScript functions associated with temperature and relative humidity calculation, the following relations are implemented:

$$T = \alpha_1 \times \left(\frac{V_T}{V_S} - \beta_1\right) \quad RH = \alpha_2 \times \left(\frac{V_{RH}}{V_S} - \beta_2\right) \quad (3)$$

where $\alpha_1 = 212.765\ ^\circ\text{C}$, $\beta_1 = 0.320$, $\alpha_2 = 210.970\ \%\ RH$, $\beta_2 = 0.235$, $V_S = +5$ V, V_T is the temperature channel's voltage, and V_{RH} is the relative humidity channel's voltage. In the GS_i case, a set of JS_{NPB_i} (JavaScript neural processing block for i measurement channel: NPB_i) functions are used.

The utilization of NPBs is related with the inverse modeling [16] of gas sensor multivariable nonlinear characteristics, which are strongly dependent on temperature and humidity but are also influenced by the concentration of other gases as part of the analyzed gas mixture. Based on the designed NPB_i, a digital readout of the gas concentration with temperature and compensation [17] is obtained.

A. NPB_i Architecture and Design

The used neural processing blocks (NPBi) are two inputs-one output multilayer perceptron neural networks (Fig. 6).

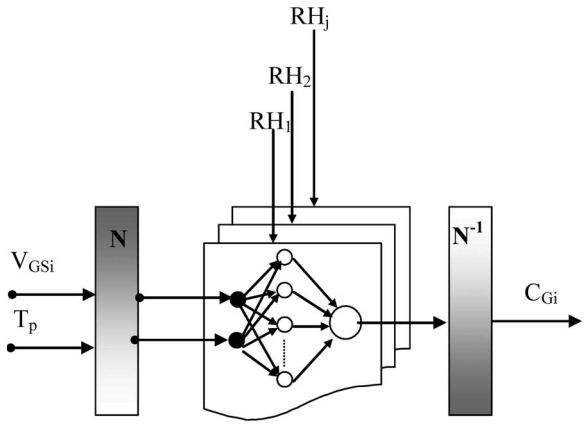

Fig. 6. The NPB$_i$ architecture. N, N^{-1}: Normalization and denormalization blocks. RH_j: Humidity selector. C_{G_i}: Temperature and humidity compensated values of the gas concentration G_i. T_P: Temperature input value. V_{GS_i}: Input voltage value on the GS$_i$ channel.

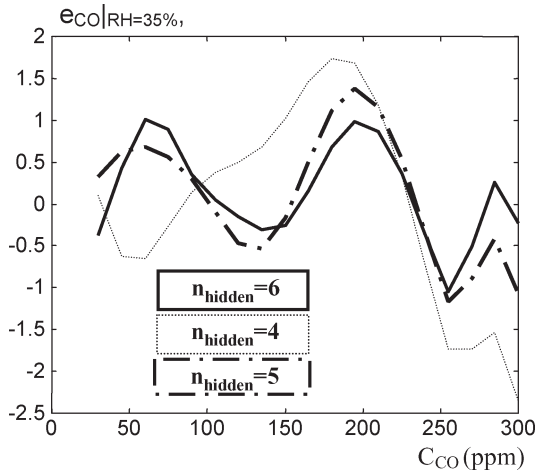

Fig. 7. Modeling error versus concentration for different NPB$_{\mathrm{CO}}$ architectures ($T = 10\ ^{\circ}\mathrm{C}$).

The NPB$_i$'s internal parameters (weights and biases) are calculated offline using MATLAB. The neural network training data were obtained in the system calibration phase. They are voltage values (V_{GS_i}) acquired from the gas concentration measurement channel for different values of gas concentration C_{G_i} and different temperature (T_p) and relative humidity (RH_i) conditions.

The developed MATLAB neural network design program calculates different sets of weights and biases for each RH_i experimental value (e.g., $RH = \{45\%, 55\%, 65\%\}$. In the air quality parameters measuring phase, the calculated weights are used by JavaScript- or LabVIEW-implemented functions for online processing of the acquired voltages.

The NPB$_i$ inputs are the normalized voltages associated with gas sensors' channels and a normalized temperature, while the NPB$_i$'s output is the temperature-compensated gas concentration C_{G_i}. The NPB$_i$ normalized inputs are defined by

$$V_{\mathrm{GS}_i}^{N} = \frac{V_{\mathrm{GS}_i}}{V1_{\mathrm{S}}} \quad T^{N} = \frac{T}{\max(T)} \tag{4}$$

where $V1_S$ represents the gas sensor normalization factor (GS$_i$ voltage supply $= +10$ V in this paper).

Because GS$_i$ characteristics depend on humidity [13], an accurate measurement of the gas concentration is provided using different NPB$_i|_{RH}$s whose weights and biases are calculated using data obtained for different relative humidity conditions (i.e., $RH = 45\%, 55\%,$ and 65%) and the interpolation method presented in [18].

The number of NPB$_i$'s layers is three. The hidden layers have two to five tansignoid (tansig(x)) neurons, and the output layer has one linear ($l(x)$) neuron. The implemented tansig(x) calculate its output according to

$$\mathrm{tansig}(x) = \frac{2}{1 + \exp(-2x)} - 1 \tag{5}$$

which leads to a reduction in the computational load.

Two criteria for NPB$_i$ design were considered, namely, the type and the number of neurons on the hidden layer, both determining the capabilities of the NPB$_i$ to adapt to a given characteristic. Different neuron nonlinear activation functions require different memory space and processing capabilities from the hardware platform. In this paper (tansignoid activation function), the neural processing task is distributed between the sensing node, which includes an embedded Web server, and the Web client (laptop PC), thus reducing the requirements of complex processing at the IPμ8930 level. At the same time, and considering the IPμ8930 memory space, an optimization of HTML number of pages and the page size was carried out.

To diminish the vector sizes of weights and biases, a study concerning the number of neurons for a required NPB$_i$ performance, which is expressed by a modeling error, was also carried out. More neurons imply complex processing but, first, imply large dimensions of the weights and biases matrices, which mean large memory requirements. Thus, the objective was to reduce the number of hidden neurons, taking into account the limited memory resources (512 kB EEPROM) of the IPμ8930 and the browser's online sensor data processing capabilities.

For the particular case of the CO measuring channel, the training set includes, as target, 15 CO concentration values uniformly distributed in the 30–300 ppm interval. The input values are the voltage values acquired from the TGS203 CO concentration measuring channel corresponding to the aforementioned concentrations. The measured temperature in the testing chamber was T_p [in degrees Celsius] $= 10 \times p$, $p = \{1, 2, 3, 4, 5\}$, and the relative humidity was $RH = 35\%$. The Levenberg–Marquardt algorithm [19] was used to calculate the weights and biases (i.e., W_{NPB_i} and B_{NPB_i}) of the neural network. Imposing a sum square error stop condition SSE $= 0.01$, and for neural networks characterized by four, five, or and hidden neurons, different measuring channel modeling error characteristics (e_{CGsi}) were obtained (Fig. 7). The modeling error is defined by

$$e_{\mathrm{CGsi}} = \frac{C_{\mathrm{CGsi}} - C_{\mathrm{CGsi}}^{\mathrm{NPB}}}{\mathrm{FS}} \times 100 \tag{6}$$

where FS represents the measurement range, C_{CGsi} is the experimental used gas concentration (e.g., CO concentration) expressed in parts per million, and $C_{\mathrm{CGsi}}^{\mathrm{NPB}}$ is the concentration of gas calculated by the corresponding neural processing module.

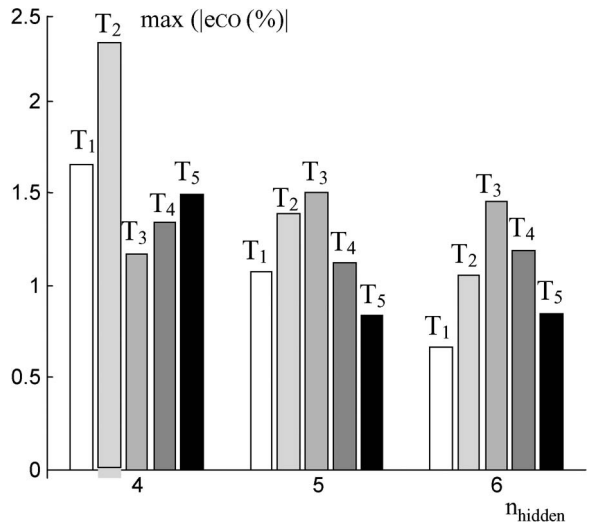

Fig. 8. Maximum inverse modeling error for different $\mathrm{NPB_{CO}}$ architectures ($n_{\mathrm{hidden}} = \{4, 5, 6\}$) and different temperatures $T_p = 10p$ °C.

Since the used gas sensors characteristic depends on temperature, a study related with the CO channel modeling error (e_{CO}) versus temperature was carried out (Fig. 8).

With humidity being an influence quantity, different values of the relative humidity lead to different primary gas selectivity characteristics and, hence, to different gas concentration measurement accuracies. Thus, experimental data obtained for three different values of relative humidity, i.e., $RH_1 = 35\%$, $RH_2 = 65\%$, and $RH_3 = 95\%$, and five values of temperatures included in the $I_T = [10; 50]$°C were considered. The imposed gas concentrations for measurement system testing were ten values of methane concentration distributed in the $I_{\mathrm{CM}} = [500; 5000]$ ppm interval, 15 values of CO concentration $I_{\mathrm{CCO}} = [30; 300]$ ppm, and 15 values of solvent vapors (ethanol vapors) concentration, i.e., $C_{\mathrm{SV}} = [50; 5000]$ ppm.

Based on the GS_i voltages for the considered gases concentrations, and taking into account temperature and humidity, three sets of weights and biases (35%, 65%, and 95% relative humidity) were calculated for CO, methane, and solvent vapor measurement channel.

B. NPB_i JavaScript Implementation

The weights and biases data are stored in numerical arrays used by the JavaScript neural processing functions $\mathrm{JSN_{AC}}$, JSN_M, $\mathrm{JSN_{CO}}$, and $\mathrm{JSN_{SV}}$ that are embedded in the APC's HTML pages.

The online JSN_i neural network processing is based on the following relation:

$$C_{G_i}^N = \sum_{q=1}^{Q} \left(w2_q \left(\frac{2}{1+\exp(\xi_i)} - 1 \right) \right) + b2 \Bigg|_{RH=RH_j}$$

$$\xi_i = -2 \times \sum_{q=1}^{Q} \left(w1_{q1} \times V_{\mathrm{GS}_i}^N + w1_{q2} \times T^N + b1_q \right) \quad (7)$$

where $w1_{q1}$ and $w1_{q2}$ are the hidden neurons weights, $b1_q$ represents the hidden neuron biases, $w2_q$ represents the output neuron weights, $b2$ is the output neuron bias, Q is the number of neurons of the hidden layer (e.g., $Q = 3$ for $\mathrm{GS_{CO}}$), V_{Gsi}^N represents the normalized values of the acquired voltage at the GS_i channel, and T^N is the normalized environment temperature. The NPB_i output is the normalized gas concentration value $(C_{G_i}^N)$ and is calculated using a set of weights and biases calculated for the RH_j closest to the measured RH value (e.g., for $RH = 42.3\%$, the weights and biases for $RH_1 = 35\%$ are used) according to the weighted selection method described in [18].

The JSN implementation uses JavaScript arithmetic operators and the JavaScript "exp" method of the JavaScript Math object. Additional implemented functions perform the sums associated with the $C_{G_i}^N$ calculation.

The technique used to send the data from the APC to JavaScript functions as parts of the HTML pages stored in the $AirQ$ node memory is based on IPμ8930 dynamic WebHoles feature [20]. Thus, every time a given HTML page (e.g., 70_AirQ_G.htm) is requested by the PC browser from the IPμ8930 Web server (e.g., http://193.136.143.205/70_AirQ_G.htm), the decimal code D_{ACH_j} associated with measuring channel j voltage (ACH_j) (e.g., 625 code corresponding to $V_{\mathrm{Gsi}} = 3$ V) is inserted into the dynamic WebHole previously configured using IPμ8930 WebHole Editor. When the sequence of preset digits "00000" (later replaced by D_{ACH_j} using dynamic WebHoles technique) is introduced into the JSN, the calculated values of gas concentration are obtained. The JS_T and JS_{RH} also use the dynamic WebHoles to calculate RH and T.

V. Data Publishing

The air quality data at each sensing node are published using APC Web server capabilities and APC–laptop PC TCP/IP communication, together with PC LabVIEW Web server capabilities.

A. APC Web Server Publishing

The capabilities of the APC Web server permits the laptop PC of the network to access dynamic webpages associated with the current values of the gases' concentrations using the browser (e.g., Internet Explorer). Thus, each APC of the network includes the main page of the distributed air quality monitoring system (Fig. 9) that includes a set of hyperlinks denominated *sensing node i* (e.g., sensing node 2). For each sensing node, the values of temperature (T_i, in degrees Celsius), relative humidity (RH, in percent), and air quality index (X_{AirQ}) are displayed.

The air quality index is calculated using the voltage value acquired from the air quality sensor channel (V_AirQ, in volts) and the value associated with clean air condition (no pollution) (V_pal, in volts) to quantify the air quality level ($X_{AirQ} = 100\%$ for no pollution and $X_{AirQ} = 0\%$ for extreme air pollution). The air quality index is expressed by the following relation:

$$X_{AirQ}(\%) = \frac{V\_pal}{V\_AirQ} \cdot 100. \quad (8)$$

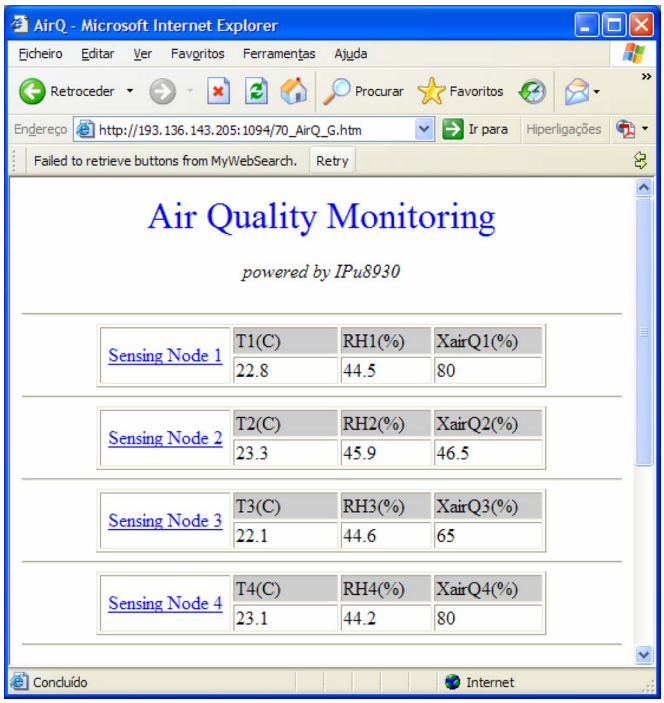

Fig. 9. Air quality monitoring webpage [T_i (in degrees Celsius), RH_i (in percent), and X_{AirQ_i} are the temperature, relative humidity, and air quality index associated with the network sensing nodes $i = 1, \ldots, 4$).

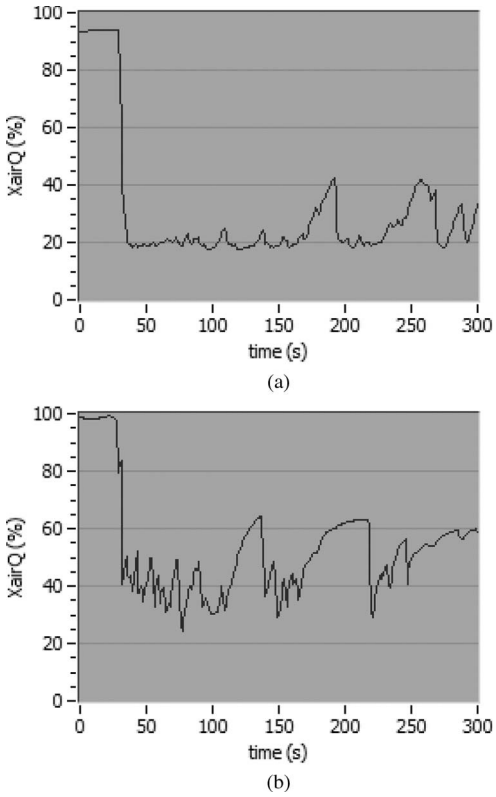

Fig. 10. Evolution of X_{AirQ} index for two home air pollution events. (a) Ethanol vapors pollution. (b) Smoke pollution.

The values of V_pal were established experimentally in a laboratory where field conditions and pollution events were simulated. Thus, values of V_pal of 1.2–1.7 V were considered for indoor clear air, i.e., when the Figaro TGS800 is used. During air quality monitoring, the V_AirQ acquired voltage is used to calculate air quality index the X_{AirQ}. Fig. 10 presents the evolution of X_{AirQ} for different pollution events.

Each hyperlink corresponds to a sensing node URL (e.g., http://193.136.143.205/74_sens2.htm), and upon selection, a detailed air quality measurement page is displayed (Fig. 11).

According to the air dynamics, the webpage refresh rate is set to a value in the 5–60 s time interval using an HTML META tag (e.g., ⟨META HTTP-EQUIV = "refresh" CONTENT = "20"⟩).

When a pollution event occurs in the area whose air quality page is displayed, an alert message "Pollution event on SN_j" is generated. The operator can click the associated button "measurement details" of the alert message to ask the Web server for detailed information, i.e., gas concentration levels (methane, CO, and solvent vapors in this paper).

Additional "pollution pages" are associated with the gas sensor measuring channels whose hyperlinks are identified in Fig. 11 by C_M, C_CO, and C_SV. These pages present the voltage values for the considered channel (e.g., V_{C_M}), the corresponding gas concentration (e.g., C_M) as a result of neural network processing, and the temperature and humidity values measured at the SN_j level. To avoid false alarms caused by anomalous functioning of the considered gas concentration measuring channel, the values obtained from general air contaminant channel (AC channel) are also used. Anomalous situations such as temperature and relative humidity that are out of range for the considered monitored region (e.g., $T = 60\ ^\circ$C and $RH = 0\%$) and false pollution alarms (expressed in high concentration values delivered by selective gas sensors, e.g., $C_M = 325$ ppm, when the AC sensor indicates low values, e.g., 10 ppm, for the same measured air) are also signaled.

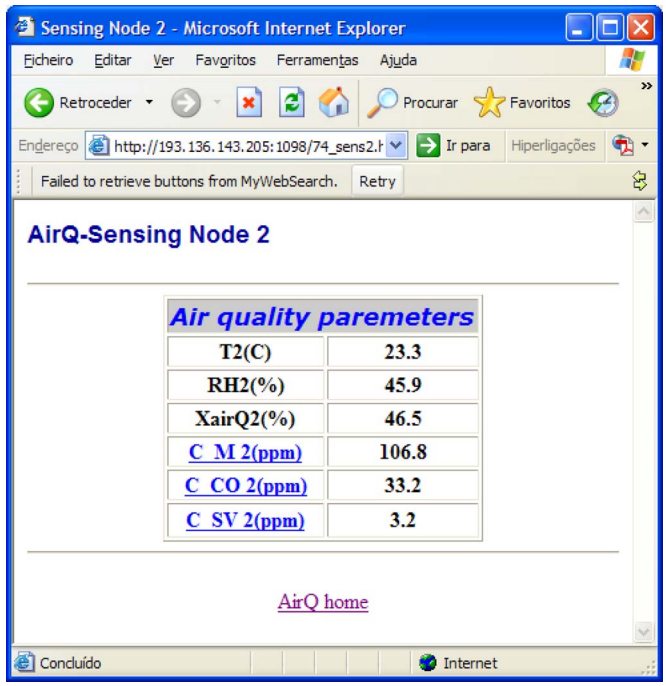

Fig. 11. Detailed air quality monitoring page—sensing node 2. T_2: Temperature value (in degrees Celsius). RH_2: Humidity values (in percent). X_{AirQ_2}: Air quality index (in percent). C_M: Methane concentration. C_CO: CO concentration. C_SV: Solvent vapors concentration.

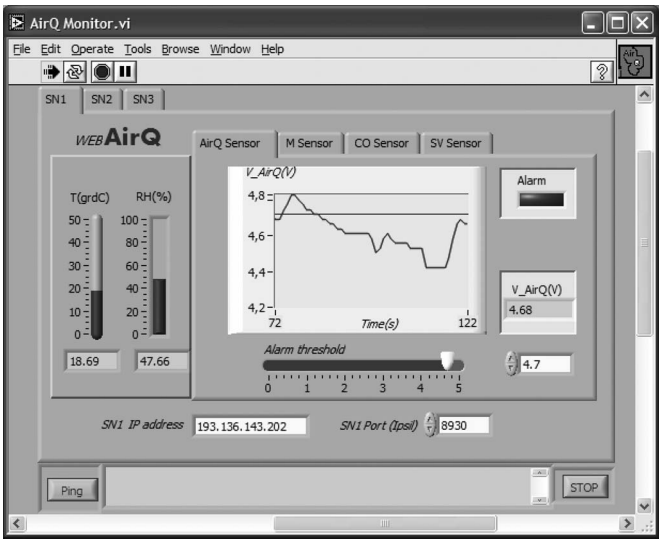

Fig. 12. GUI of the air quality monitoring system.

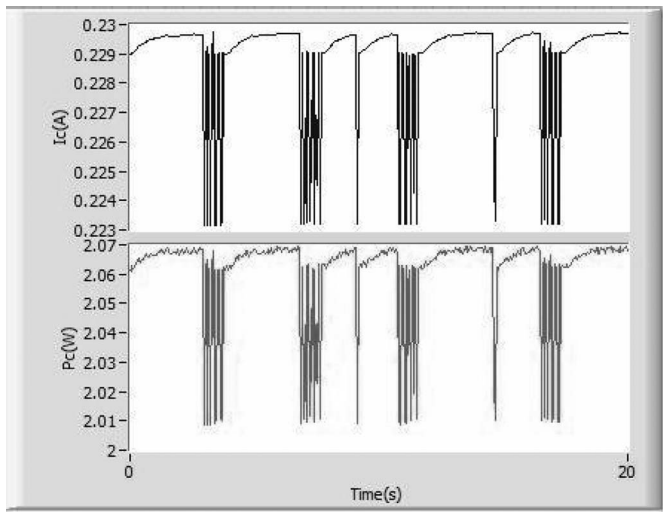

Fig. 13. SN_i and GS_{j_i} current and power consumption (I_c and P_c) evolution versus time for a main webpage refresh rate of 5 s.

B. APC LabVIEW Web Server Publishing

To perform advanced data processing and data logging tasks, a TCP/IP communication based on the LabVIEW TCP/IP function was also implemented. Using the LabVIEW software implemented in the PC, the V_{Gsi} values are accessed from the sensing nodes (SN_j) and are processed and stored in data logging files, which permits us to obtain the historical evolution of the air quality in the monitored areas and to evaluate air quality trends. Fig. 12 shows the graphical user interface (GUI) associated with SN_i's channel monitoring.

In the figure, one can observe that together with voltage levels associated with air quality sensors, the values of temperature (T) and relative humidity are also displayed. At the same time, pollution events are signaled if the ITGS800 output voltage exceeds the imposed alarm threshold (4.7 V in this paper, which corresponds to an ethanol concentration of 10 ppm). Elements of IP address and port are included on the SN_i's configuration panel.

The implemented interface permits us to check the laptop PC–SN_i network communication using the *ping* function.

VI. Power Requirements

To characterize the power required by the wireless network for air quality monitoring, a general-purpose-interface-bus-based virtual system that includes a set of Agilent 34401A multimeters used to evaluate the dissipated power through the measurement of current and voltage at SN_i, GS_{j_i}, and WB_i levels was developed.

A. SN_i and GS_{j_i} Power Dissipation

The SN_i power dissipation evaluation was studied according to the different measurement tasks considering different numbers of active sensors. Thus, under normal conditions (nonoccurrence of pollution event), only the temperature, relative humidity, and air quality sensors are active. The $\mathrm{SN}_i{-}\mathrm{GS}_{j_i}$ associated power consumption is $P_{\mathrm{SN\_GS}_{j_i}} = 2.05$ W for a voltage supply $V_s = +9$ V.

The second group of measurements is related to $\mathrm{SN}_i{-}\mathrm{GS}_{j_i}$ power dissipation for different working cases (e.g., continuous acquisition with Web publishing and continuous acquisition with TCP/IP data communication based on LabVIEW). Some results are presented in Fig. 13.

As shown in Fig. 13, and considering an air quality webpage refresh rate $t_{\mathrm{refresh}} = 5$ s, the fluctuation of the consumed power $P_c = P_{\mathrm{SN}_i} + P_{\mathrm{GS}_{j_i}}$ is about 59 mW. This fluctuation can be associated with data acquisition and dynamic webpage publishing. When the SN_i only acquires the sensor channel voltages and transmits data to the laptop PC (through IEEE803.11b using the DWL-810+ wireless bridge) to be processed and published using the LabVIEW Web server capabilities, the average power consumption $P_{C\text{-PC}}$ is about 98% of P_C. Thus, from the power consumption point of view, the two webpage presentation solutions are equivalent.

The used gas sensors are important power consumers of the considered network. Thus, in general air monitoring mode (nonpollution event) when only the TGS800, temperature, and relative humidity sensors are switched on, the power consumption average corresponds to the $P_{\mathrm{SN\_GS}_{j_i}}$ aforementioned value. Inducing a pollution event (e.g., 400 ppm ethanol), the power consumption associated with air quality sensor is shown in Fig. 14.

After pollution event detection through general air quality sensor, all the SN_i's gas sensors are activated, which leads to about 4×1.24 W GS_{j_i} power consumption. The GS_{j_i} power consumption is part of the total power consumption that includes the SN_i and WB_i consumption.

B. WB_i Power Dissipation

The wireless communication is a major power consumer during system operation. On power-on active state mode, the used wireless bridge average power dissipation (P_{WB_i}) is about 3.14 W. When the link between the SN_i and WB_i is

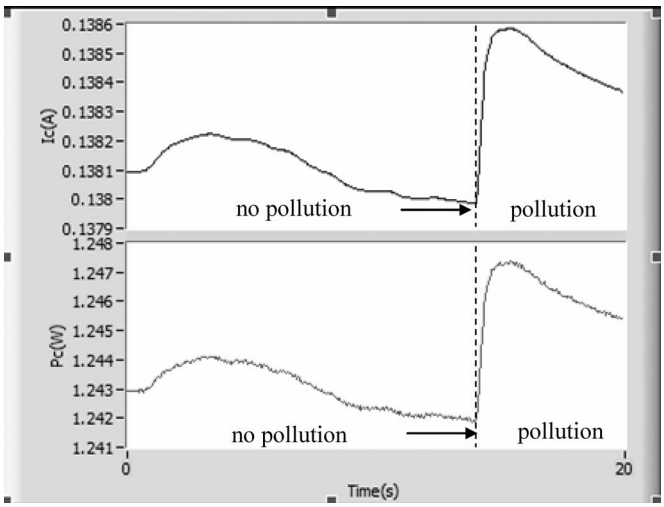

Fig. 14. TGS800 power consumption with and without a pollution event.

established, P_{WB_i} reaches 3.58 W. This value is due to the TCP/IP communication between the SN_i and the laptop PC through the implemented WLAN.

VII. Conclusion

This paper has reported the implementation of a measuring system for air quality monitoring. Two architectures are proposed for wireless communication between the sensing nodes and a personal computer that manages the whole system. Because of the communication range of the hardware used, the systems are particularly suited for indoor applications. The outdoor range limitation can be overcome using high-gain omnidirectional antennas (e.g., D-Link ANT24-1500) that provide extended coverage for an existing 802.11b/g wireless network avoiding the cost and complexity of adding additional wireless APs or wireless repeaters. The coverage of the Wi-Fi designed network can be extended up to tens of kilometers by including in the system extended coverage Wi-Fi repeaters (e.g., Duganit WL-2410).

Considering the increasing number of the low-cost or even free Wi-Fi Internet hotspots and the capabilities of the distributed air-quality-developed system (based on air-quality-embedded Web sensors), different locations can be monitored and the air quality values Web published as long as they have Wi-Fi coverage.

The output of the used gas sensors depends not only on the cross influence of the primary measured gas but also on external influence factors, namely temperature and humidity. Thus, several NPBs were implemented to obtain the temperature and humidity corrected values of the gases' concentrations. The merits of this type of technique for the required purpose, i.e., the accurate inverse modeling of the gas measuring channel for a small number of calibration points, are well established.

The main novelties of this paper are given as follows: 1) the development of an air quality monitoring system that uses smart sensors in a wireless network; 2) the embedding of neural network processing blocks distributing the processing charge between the embedded systems (Web sensor) and the Web browser installed in a personal computer; and 3) the development of PC software for sensing node TCP/IP remote control, advanced data processing, data storage, and Web publishing software associated with air quality monitoring system. Special attention was granted to the optimal implementation of the neural network and to a practical evaluation of the distributed sensing system power consumption.

The proposed air quality monitoring system based on a wireless smart sensor network and on neural network processing blocks embedded on the sensing nodes' HTML pages presents the following advantages.

- It provides extended capabilities for air quality monitoring for indoor and outdoor conditions.
- It provides good accuracy of gas concentration measurements by using neural networks to compensate the temperature and humidity influences.
- It presents a client-side JavaScript solution for neural network implementation.
- Based on TCP/IP read and write functions implemented in LabVIEW, it allows advanced processing of air quality data by a PC.

Measurements of the system's power requirements show that each node requires about 8 W. This clearly indicates that a system's autonomy of days or months can only be reached if batteries' recharge capability, using, for instance, solar panels, is provided.

The output of a specific tin dioxide sensor arrays depends not only on temperature and humidity but also on the concentration of other gases and vapors. The effect of this cross influence on the accuracy of the measurement can be minimized using also neural networks. We will address this problem in a future work.

References

[1] European Environment Agency, *Air Pollution*, 2001. Report.
[2] J. Bartolomeo, "Detecting CO in the home," *Home Automation and Building Control*, pp. 51–55, Oct. 1995.
[3] *Nemoto Chemical Sensors Catalogue*, Nemoto & Co., Tokyo, Japan. [Online]. Available: http://www.nemoto.co.jp/product
[4] F. Sarry and M. Lumbreras, "Gas discrimination in an air-conditioned system," *IEEE Trans. Instrum. Meas.*, vol. 49, no. 4, pp. 809–812, Aug. 2000.
[5] S. Marco, A. Ortega, A. Pardo, and J. Samitier, "Gas identification with tin oxide sensor array and self-organizing maps: Adaptive correction of sensor drifts," *IEEE Trans. Instrum. Meas.*, vol. 47, no. 1, pp. 316–320, Feb. 1998.
[6] A. Lee and B. Reedy, "Temperature modulation in semiconductor gas sensing," *Sens. Actuators B, Chem.*, vol. 60, no. 1, pp. 35–42, Nov. 2, 1999.
[7] F. Ménil, M. Susbielles, H. Debéda, C. Lucat, and P. Tardy, "Evidence of a correlation between the non-linearity of chemical sensors and the asymmetry of their response and recovery curves," *Sens. Actuators B, Chem.*, vol. 106, no. 1, pp. 407–423, Apr. 29, 2005.
[8] R. Selmic and F. L. Lewis, "Neural-network approximation of piecewise continuous functions: Application to friction compensation," *IEEE Trans. Neural Netw.*, vol. 13, no. 3, pp. 745–751, May 2002.
[9] H. G. Ramos, J. M. Dias Pereira, V. Viegas, O. Postolache, and P. M. B. Silva Girão, "A virtual instrument to test smart transducer interface modules (STIMs)," *IEEE Trans. Instrum. Meas.*, vol. 53, no. 4, pp. 1232–1239, Aug. 2004.
[10] *IEEE Std. 1451.2-1997, Standard for a Smart Transducer Interface for Sensors and Actuators—Transducer to Microprocessor Communication Protocols and Transducer Electronic Data Sheet (TEDS) Formats*, Sep. 25, 1998, New York: IEEE. #SH94566.
[11] J. M. Dias Pereira, P. M. B. Silva Girão, and O. Postolache, "Fitting transducer characteristics to measured data," *IEEE Signal Process. Mag.*, vol. 4, no. 4, pp. 26–39, Dec. 2001.

[12] M. Gast and M. S. Gast, *802.11 Wireless Networks: The Definitive Guide*. Sebastopol, CA: O'Reilly, 2002.
[13] *Gas Sensors Catalog*, Figaro, Osaka, Japan. [Online]. Available: http://www.figaro.co.jp/en/make_html/item_1.html
[14] Smartec, *Smartec-Sensors Catalog*. [Online]. Available: http://www.mmselectronics.co.uk/smt160-30.htm
[15] *Relative Humidity Sensor-HS1100*, Humirel Inc., Chandler, AZ, 1999.
[16] J. Patra, A. Kot, and G. Panda, "An intelligent pressure sensor using neural networks," *IEEE Trans. Instrum. Meas.*, vol. 49, no. 4, pp. 829–834, Aug. 2000.
[17] O. Postolache, M. Pereira, P. M. B. Silva Girão, M. Cretu, and C. Fosalau, "Application of neural structures in water quality measurements," in *Proc. IMEKO World Congr.*. Wien, , Austria, Sep. 2000, vol. IX, pp. 353–358.
[18] J. Pereira, O. Postolache, and P. M. B. Silva Girão, "A temperature-compensated system for magnetic field measurements based on artificial neural networks," *IEEE Trans. Instrum. Meas.*, vol. 47, no. 2, pp. 494–498, Apr. 1998.
[19] M. T. Hagan and M. B. Menhaj, "Training feedforward networks with the Marquardt algorithm," *IEEE Trans. Neural Netw.*, vol. 5, no. 6, pp. 989–993, Nov. 1994.
[20] *IPμ8930 Developer Guide*, Ipsil, Bethesda, MD. [Online]. Available: www.ipsil.com

Octavian A. Postolache (SM'06) was born in Piatra Neamt, Romania, on July 29, 1967. He received the Ph.D. degree in electrical engineering from the "Gh. Asachi" Technical University of Iasi, Iasi, Romania, in 1999.

In 1992, he joined the Faculty of Electrical Engineering, Department of Electrical Measurements and Electrical Materials, Technical University of Iasi, where he was a Lecturer and an Assistant Professor for nine years. In 2000, he joined the Instituto Superior Técnico, Lisbon, Portugal, and the Instituto de Telecomunicações, Lisbon, as a Ph.D. Researcher, where he has been involved in different projects in the area of instrumentation. His main research interests included smart sensors for environmental and biomedical applications, distributed instrumentation, sensor networks, and computational intelligence implementation in automated measurement systems.

J. M. Dias Pereira (SM'05) was born in Portugal in 1959. He received a 5-year degree in electrical engineering (Licenciatura) and the M.Sc. and the Ph.D. degrees in electrical and computer engineering from the Technical University of Lisbon, Lisbon, Portugal, in 1982, 1995, and 1999, respectively.

During almost eight years, he was with Portugal Telecom, working on digital switching and transmission systems. In 1992, he returned to Escola Superior de Tecnologia, Instituto Politécnico de Setúbal, Setúbal, Portugal, as an Assistant Professor, where he is currently a Coordinator Professor. He is also with the Instituto de Telecomunicações, Lisbon. His main research interests include instrumentation and measurements.

P. M. B. Silva Girão (SM'01) was born in Lisbon, Portugal, on February 27, 1952. He received the Ph.D. degree in electrical engineering from the Technical University of Lisbon (UTL) in 1988.

In 1975, he joined the Department of Electrical Engineering, Instituto Superior Técnico, UTL, as a Lecturer. In 1997, he joined the Instituto de Telecomunicações, where he is currently a Senior Researcher, the Head of the Instrumentation and Measurements Group, and a Coordinator of the Basic Sciences and Enabling Technologies scientific area. He is a member of the Editorial Boards of *Measurement* (Elsevier), the TRANSACTIONS ON SYSTEMS, SIGNALS AND DEVICES (Shaker-Verlag), and the *Sensors and Transducers Journal*. His current main research interests include instrumentation, transducers, measurement techniques and digital data processing, particularly for biomedical, environmental, chemical, and civil applications. Metrology, quality, and electromagnetic compatibility are also areas of his regular activity, mainly as an Auditor for the Portuguese Institute for Quality (IPQ).

Prof. Girão is a member of the Editorial Board of the European Commission External Expert for Evaluation and Assessment of Proposal and Projects, a regular reviewer of several international scientific publications, the Chairman of IMEKO TC19—Environmental Measurements, and the Vice President of the Portuguese Metrology Society.